JOURNAL OF PROPULSION AND POWER
Vol. 11, No. 6, November–December 1995

Shock-Wave/Boundary-Layer Interactions with Bleed Part 1: Effect of Slot Angle

A. Hamed,* J. J. Yeuan,† and S. H. Shih‡
University of Cincinnati, Cincinnati, Ohio 45221

The effect of bleed configuration in the interaction region of an oblique shock wave and a turbulent boundary layer was investigated using numerical simulations. The numerical solution is obtained for the compressible Navier–Stokes and k-ε equations throughout the interaction zone and inside the slanted and normal bleed slots. Different bleed mass flow rates, up to 16% of the incoming boundary layer, are obtained by varying the bleed slot outflow face pressure. Results are presented for an incident oblique shock of sufficient strength to cause boundary-layer separation in the absence of bleed. The results show the flow characteristics including an expansion/compression wave system across the slot opening and recirculation zone inside the slot. The performance of the different bleed configurations is compared in terms of the discharge coefficient and the boundary-layer characteristics downstream of the interaction, over a range of bleed mass flow rates. In Part 1, results are presented for bleed applied across the shock impingement point through slots at 20-, 30-, 40-, and 90-deg angles to the plate surface. The results indicate considerable change in the flow characteristics inside the bleed slot with the slant angle. The bleed discharge coefficient increased as the slot slant angle decreased. The plate surface friction coefficient downstream of the interaction was much lower in the case of bleed through normal slots than slanted slots where it had the characteristics of redeveloping boundary layer.

Introduction

EXPERIMENTAL investigations of bleed (suction) in supersonic flowfields[1] have been conducted to characterize the bleed flow[2–4] and its effect on the boundary layer.[5–11] Syberg and Koncsek[2] represented supersonic inlet test data from Refs. 3 and 4 in the form of bleed drag and mass flow coefficient. These bleed data were obtained in supersonic flows without shock interactions in the bleed zone and with fully developed boundary layers upstream of the bleed region. The data that were obtained over a range of Mach numbers show the effects of bleed hole size, slant angle, and length-to-diameter ratio. Bleed holes at 20 deg to the surface had higher flow coefficient and could be operated at a higher plenum pressure than the 40- and 90-deg holes.[2] The bleed mass flow increased and drag decreased as the external Mach number increased. Pitot pressure surveys of boundary-layer characteristics upstream and downstream of the shock-wave/boundary-layer interactions were obtained by Fukuda et al.[5] and Wong[6] across the interaction regions in supersonic inlets, by Seebaugh and Childs[7] on a cylindrical surface, and by Benhachmi et al.,[8] Hingst and Tanji,[9] Lee and Leblanc,[10] and Strike and Rippy[11] on a flat plate. The conclusions regarding the effects of bleed hole size[5,6] and bleed location relative to the shock[5,7,9,11] on the boundary layer downstream varied among the different studies. The discrepancies among the different experimental studies is an indication of the complexity of the flow in these configurations. Based on the comparison of their computational results with the experimental data of supersonic inlet flowfields, Reddy et al.[12] stressed the need for a detailed study of the effect of the individual bleed ports. Bleed optimization can only be accomplished through a parametric investigation in which the bleed conditions are changed systematically. The large number of parameters and the difficulties in obtaining accurate flow measurements in the interaction zone precludes a complete experimental investigation.

Recently, a number of numerical studies have been aimed at investigating shock-wave/boundary-layer interactions with bleed. Paytner et al.,[13] Benhachmi et al.,[8] and Abramson et al.[14] simulated the hole roughness effects in their numerical solutions to the Navier–Stokes equations, using Cebeci's algebraic turbulence model for rough wall.[15,16] In this approach, the solution provides the boundary-layer characteristics downstream, but not the mass flow distribution across the bleed zone that are specified as a boundary condition in the numerical solution. Remlinger et al.[17] and Hamed et al.[18–21] modeled bleed by resolving the flow through the individual bleed ports. The advantage of this approach is that the mass flux distribution, bleed drag, as well as the boundary-layer characteristics downstream can be determined from the numerical solution. Comparative information regarding the effect of bleed hole size, slant angle, and bleed location relative to the shock obtained using this approach can therefore be used to help resolve the discrepancies among the different experimental data. For bleed through a normal slot, Hamed et al.[19] investigated the effects of bleed location[19] and slot width and depth[20,21] on the flowfield in the interaction zone of an oblique shock-wave/boundary-layer interaction. The results obtained in these investigations for shock strength sufficient to cause flow separation with no bleed indicate that slot width equal to or greater than the incoming boundary-layer thickness was required to eliminate turbulent boundary-layer separation by removing 20–30% of the incoming boundary-layer mass flow. Across the shock bleed location was most effective in eliminating separation.

The purpose of the present study is to characterize the flowfield in oblique shock-wave/turbulent boundary-layer interactions with bleed through slanted slots. In the investigated configuration, flow suction (bleed) is applied across the incident oblique shock location on a flat plate turbulent boundary layer through slots slanted at different angles relative to the surface. The results show the effect of the slant angle on

Presented as Paper 93-2155 at the AIAA/SAE/ASME/ASEE 29th Joint Propulsion Conference and Exhibit, Monterey, CA, June 28–30, 1993; received Aug. 6, 1994; revision received Jan. 27, 1995; accepted for publication Feb. 11, 1995.

*Professor, Department of Aerospace Engineering and Engineering Mechanics. Fellow AIAA.
†Postdoctoral Assistant, Department of Aerospace Engineering and Engineering Mechanics. Member AIAA.
‡Student, Department of Aerospace Engineering and Engineering Mechanics. Student Member AIAA.

the bleed slot discharge coefficient, total pressure recovery, and on the boundary-layer characteristics downstream of the interaction at the different bleed mass flow rates up to choked conditions.

Analysis

The partial differential equations used to describe the flow are the full two-dimensional compressible Navier–Stokes equations in strong conservation form and general curvilinear coordinates. The PARC code[22] was used in the numerical solution with a two-equation turbulence model based on Chien's low Reynolds number k-ε model[23] with Nichols'[24] modifications to add compressibility effects. The flow was considered to be turbulent throughout and no attempt was made to model transition or relaminarization. Figure 1 shows the solution domain used in the two-dimensional flow simulations. It extends upstream of the flat plate leading edge, downstream of the shock-wave/turbulent boundary-layer interaction region, and inside the bleed slot. The specified plenum outflow face pressure controls the amount of bleed mass flow. The incident oblique shock crosses the upper boundary, and all other wave systems including the reflected, and any separation and reattachment shocks cross the outflow boundary. The location of the incident shock is fixed at the upper boundary with freestream and postshock conditions specified upstream and downstream. Uniform freestream flow conditions are applied at the inflow boundary and all variables were extrapolated at the outflow boundary. No-slip adiabatic flow conditions are applied at the plate and bleed walls. The static pressure is specified and first-order extrapolation is applied for the rest of the flow variables at the bottom of the bleed slot. The slot was always centered around the shock impingement location at 1 ft from the flat plate leading edge.

Referring to Fig. 1, the computations were performed using a 308 × 68 grid over the plate surface and an 89 × 68 grid inside the bleed slot. Variable grid spacing was used in both x and y directions for grid clustering around the bleed walls and at the plate surface, with $y_{min} = x_{min} = 0.2579410^{-4}$ ft corresponding to $y^+ = 2.0$ at $x = 0.9$ ft. Computations for a typical bleed case required 5000 local time steps at 0.2 Courant–Friedrichs–Lewy number to reach steady-state solution based on six orders of magnitude reductions in the averaged rms error in the flux.

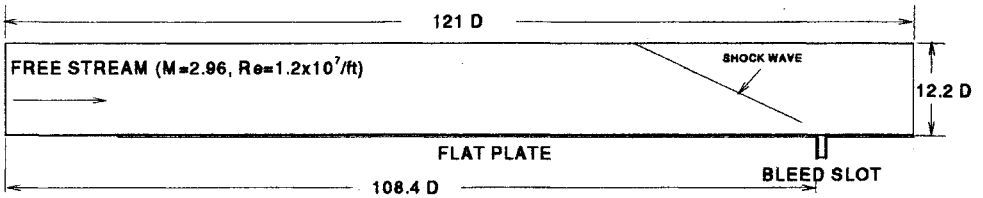

Fig. 1 Schematic of computational domain.

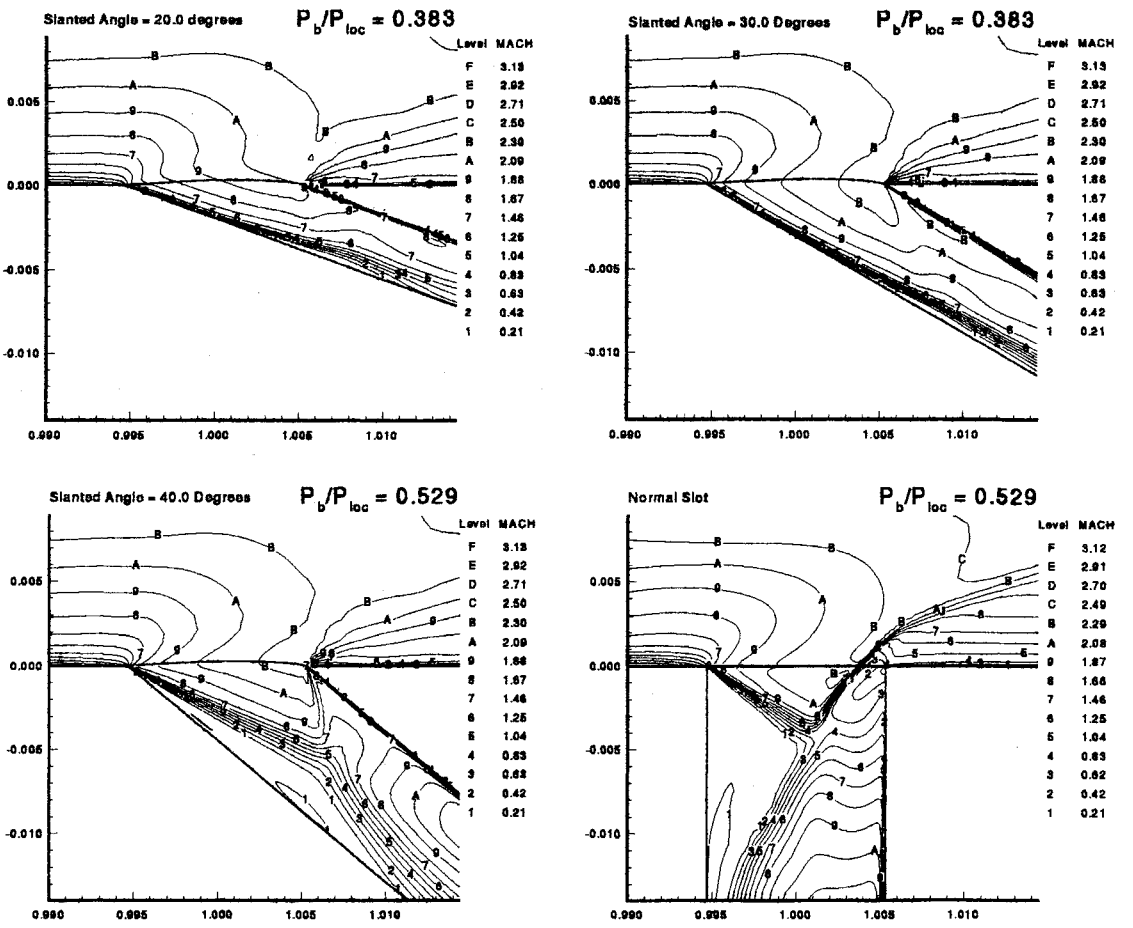

Fig. 2 Mach number contours for four different slot geometries at choked conditions.

Results and Discussion

The computations were conducted at the incoming flow conditions of $M = 2.96$, $Re = 1.2 \times 10^7$/ft, and an impinging oblique shock angle of 25.84 deg (wedge angle of 7.93 deg) corresponding to the separated flow case with no bleed.[21] The flow characteristics inside the bleed slot and throughout the interaction were determined for bleed through slanted slots at 20, 30, and 40 deg to the plate surface and for normal (90-deg) bleed. The slot width for the normal bleed case was 0.01065 ft, which is equal to 0.8085 times the boundary-layer thickness upstream of the interaction. To maintain comparable bleed mass flows among the normal and the different slanted bleed cases, the opening at the plate surface was maintained at 0.0106 ft in all cases while the slot width changed with the sine of the slant angle, leading to D/δ ratios of 0.2766, 0.4039, and 0.5202 for the 20-, 30-, and 40-deg slanted slots, respectively.

Figure 2 presents the Mach number contours for the four different slot geometries at choked conditions. The corresponding static pressure, Mach number, and flow angle distribution across the slot opening are presented in Figs. 3–5. The contours reveal a complex wave system across the slot opening starting with an expansion fan at the upstream slot corner, then an oblique shock at the downstream corner of the slanted bleed slots or a bow shock that originates inside the normal slot. The effect of this bow shock is depicted as a sharp rise in the static pressure across the normal slot opening at the plate surface as shown in Fig. 3.

A recirculating flow region inside the slot at the upstream wall is observed in all cases. Its size and location depends on the slant angle. The separated flow region occupies more than 50% of the slot width in the case of normal bleed and is reduced with increased slanting to less than 20% of the slot width, in the case of 20-deg slot. The results in Figs. 2–5 suggest that the formation of the recirculation region is controlled by two flow mechanisms. One is insufficient flow turning into bleed slot and the other is the shock wave generated at the downstream edge of the bleed slot, crossing the slot passage and impacting the upstream slot wall. The first mechanism dominates the normal and 40-deg slanted bleed cases in which the flow separates close to the upstream wall corner near the plate. The second flow mechanism affects the 20- and 30-deg slanted bleed cases where the separated flow region on the upstream bleed wall is observed inside the slot. Further insight is gained by examining the flow angle distributions across the slot opening (Fig. 5). The results in this figure suggest that only in the case of the low 20-deg angle is the flow turning into the slot limited by the bleed slot angle. Generally, lower static pressures (Fig. 3), higher Mach numbers (Fig. 4), and higher flow turning angles (Fig. 5) are predicted across the slot opening for the other configurations. However, the flow angles in the case of 30-, 40-, and 90-deg bleed slots are smaller than the physical slot angle. The difference is associated with the separation bubble inside the slot at the upstream upper corner.

According to Fig. 5, the normal slot initially generated 36-deg turning flow angle at the upstream corner, which quickly settled to an average angle of approximately 30 deg. This is caused by a small separation bubble on the plate surface up-

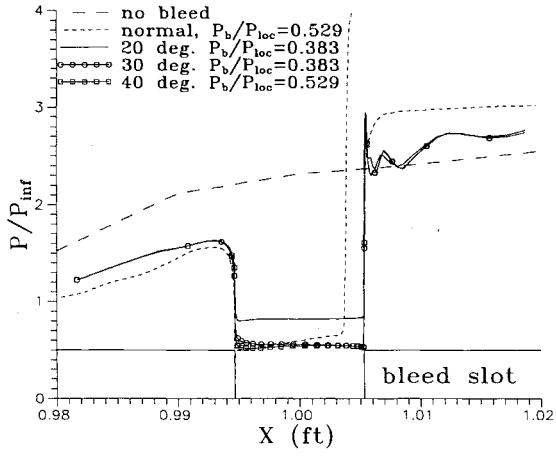

Fig. 3 Static pressure distribution across the slot opening at choked conditions.

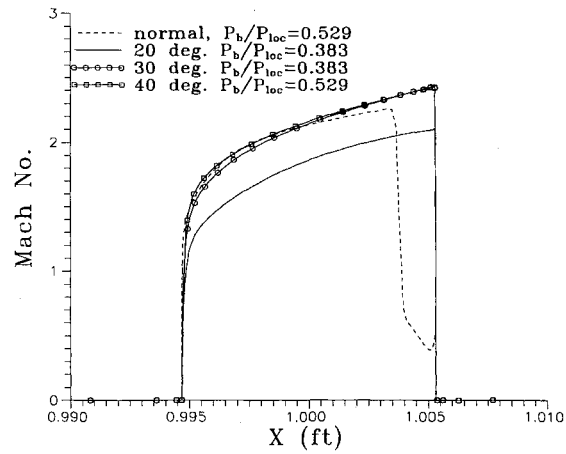

Fig. 4 Mach number distribution across the slot opening at choked conditions.

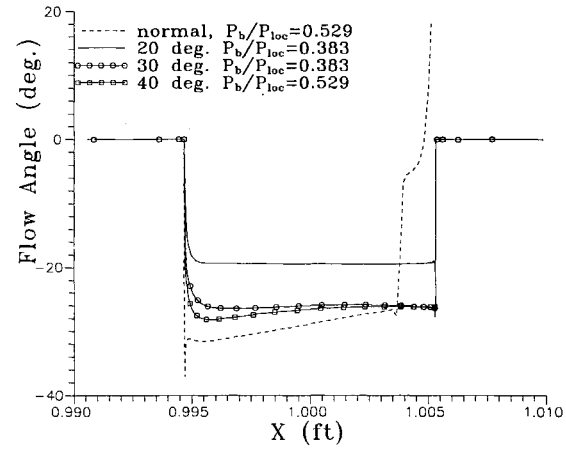

Fig. 5 Flow angle distribution across the slot opening at choked conditions.

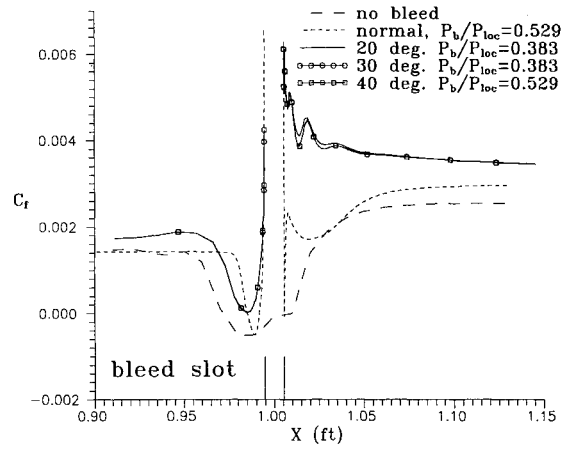

Fig. 6 Friction coefficient distribution in the interaction region at choked conditions.

stream of the slot that is confirmed by the negative friction in Fig. 6.

Figure 6, which presents the skin friction distribution over the plate surface, indicates that flow separation (negative friction coefficient) in the no-bleed case extends over a 0.04-ft region. A very small separated flow region (less than 0.01 ft) is predicted in the normal bleed case over the plate surface upstream of the slot and an even smaller one at the downstream corner. No plate surface flow separation was predicted in the three cases of slanted bleed.

The effect of boundary-layer mass removal extends both upstream and downstream of the bleed slot and affects both surface pressure and friction coefficient as can be seen in Figs. 3 and 6. The pressure rise downstream of the bleed slot is more rapid in the normal bleed case. The change in the friction coefficient over the plate surface downstream of the slanted slots is characteristically of redeveloping boundary layer. In the case of normal bleed, the skin friction initially reaches slight negative values over the plate near the normal slot's downstream corner before it eventually starts to increase further downstream.

Figure 7 presents the variation in the discharge coefficient with the plenum pressure that is normalized by the inviscid pressure P_1 behind the incident shock ($P_1/P_{inf} = 1.7752$). The same data is represented in Fig. 8 in the form of bleed mass flow as a percentage of the boundary-layer mass flow upstream of the interaction at $X = 0.9$ ft. According to these figures, the low-angle slots reach higher discharge coefficient at choking, but for the same opening at the plate surface, the maximum bleed mass flows as a percentage of the incoming boundary layer is slightly lower for the 20-deg slot bleed than for the 30-, 40-, and 90-deg slot bleed. The plenum pressure at which bleed flow initiates is low for the low-angle slot and higher for the normal bleed slot. Reference 2 presented experimental data for bleed through 20- and 30-deg slanted and normal holes over a range of freestream Mach numbers without incident shock. The data suggests that as the plenum pressure is reduced, the bleed mass flow in the 20- and 30-deg holes remain unchanged, then it drops sharply at a given

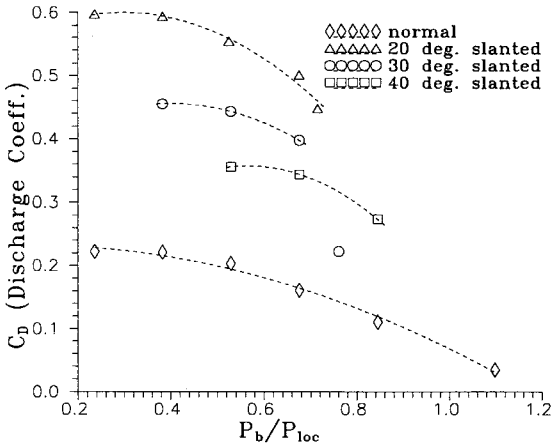

Fig. 7 Variation of discharge coefficient with the bleed plenum pressure.

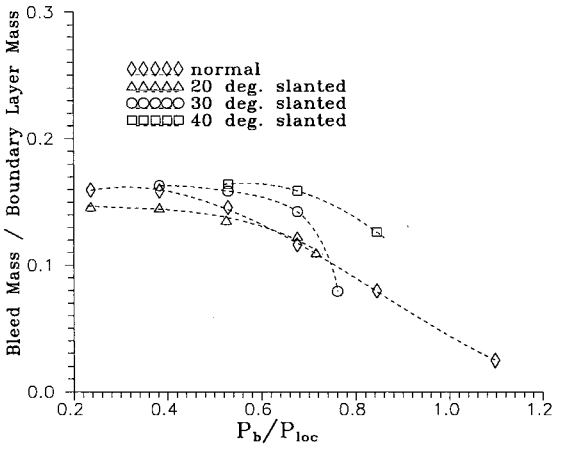

Fig. 8 Variation of bleed mass flow rate with the bleed plenum pressure.

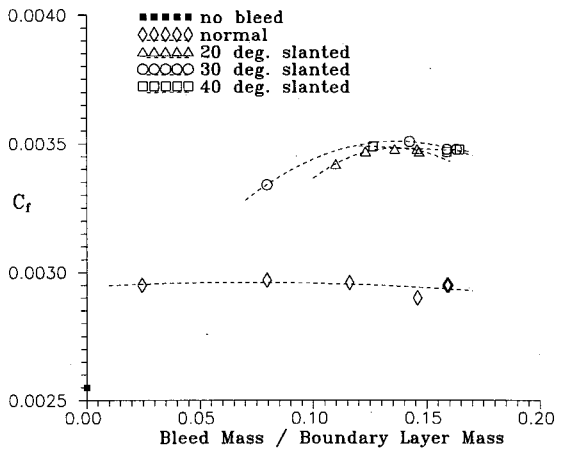

Fig. 9 Effect of bleed mass flow on the friction coefficient downstream of interaction region, at $x = 1.13$ ft.

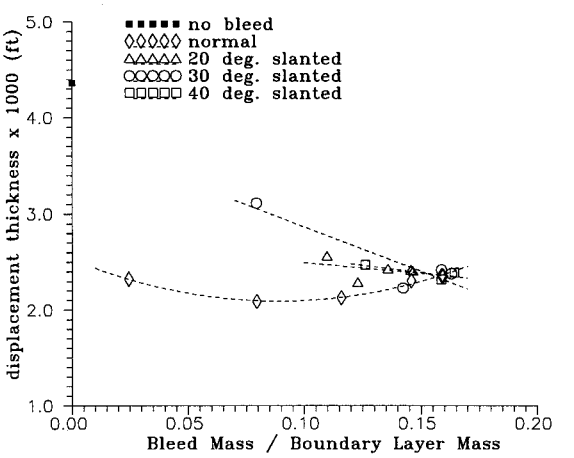

Fig. 10 Effect of bleed mass flow on the displacement thickness downstream of interaction region, at $x = 1.13$ ft.

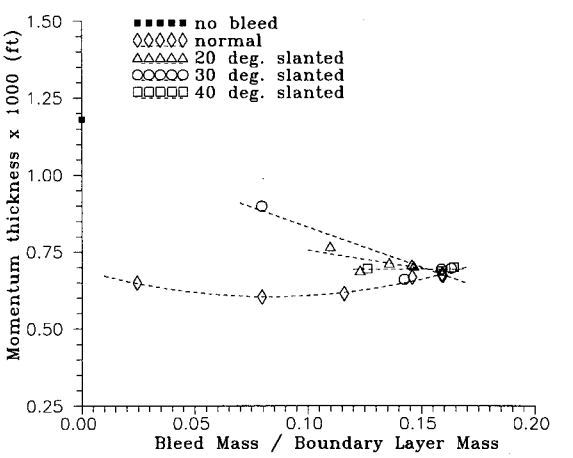

Fig. 11 Effect of bleed mass flow on the momentum thickness downstream of interaction region, at $x = 1.13$ ft.

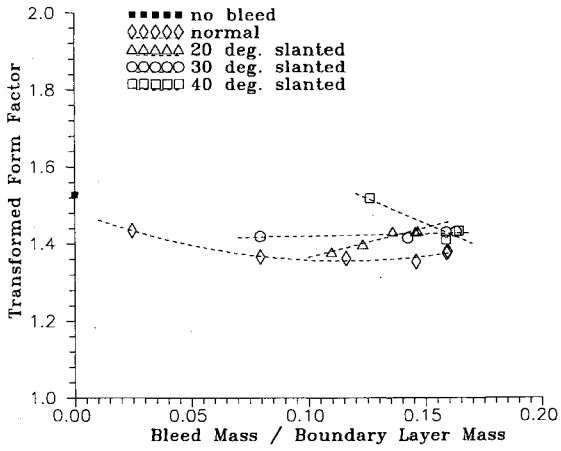

Fig. 12 Effect of bleed mass flow on the transformed form factor downstream of interaction region, at x = 1.13 ft.

value of the pressure that depends on the freestream Mach number. Since the bleed mass flow variation was accomplished in the numerical simulations by changing the bleed slot's outflow surface pressure, the ability to simulate nonchoked slanted bleed was limited to near choking values. This was not the case for bleed through normal slots where the discharge coefficient decreases more gradually with the increased plenum pressure in the case of normal bleed.

Figures 8–12 show the effect of bleed mass flow on the friction coefficient, displacement and momentum thickness, and transformed form factor downstream of the interactions at x = 1.13 ft. According to this figure, all slot configurations produce nearly the same boundary-layer displacement thickness of approximately 0.0024 ft and of boundary-layer momentum thickness of 0.0007 ft at choking. The normal bleed slot, however, produces larger reductions in the displacement thickness to 0.002 and transformed form factor to 1.36.

Conclusions

A numerical investigation was conducted to study the effect of bleed mass flow and slot slant angle on the flowfield in an oblique shock-wave/turbulent boundary-layer interaction. The results for bleed-through slots located across the shock impingement point indicate that the choked discharge coefficient increases as the bleed slot angle to the plate surface decreases. Consequently, less bleed hole area is required for the same bleed mass flow as the bleed hole slant angle decreases. However, for the same slot opening at the plate surface, the bleed mass flow approaches the same choking value of approximately 16% of the boundary layer's before the shock for the 30-, 40-, and 90-deg bleed slots. Since the flow turning into the slot is limited by the slot angle in the case of 20-deg bleed, the corresponding choking mass flow is slightly lower at 14.5% of the boundary-layer mass flow before the shock. A major difference is observed in the plate surface friction coefficient downstream of the interaction, between the slanted and normal bleed slot cases. In the first case, the friction coefficient is higher and its variation along the plate surface downstream of the slot is characteristically that of a redeveloping boundary layer. In the case of normal bleed, after reaching a negative value due to the small separation bubble on the plate surface at the downstream corner of the slot opening, the friction coefficient quickly increases and decreases again to reach that of the no-bleed case before increasing slightly further downstream.

Acknowledgments

This work was sponsored by AFOSR Contract 91-0101, L. Sakell, Project Monitor. The computational work was performed on the Cray Y-MP of the Ohio Supercomputer.

References

[1]Hamed, A., and Shang, J., "Survey of Validation Data Base for Shock Wave Boundary Layer Interactions in Supersonic Inlets," *Journal of Propulsion and Power*, Vol. 7, No. 4, 1991, pp. 617–625.

[2]Syberg, J., and Koncsek, J. L., "Bleed System Design Technology for Supersonic Inlets," AIAA Paper 72-1138, June 1972.

[3]McLafferty, G., and Ranard, E., "Pressure Losses and Flow Coefficients of Slanted Perforations Discharging from Within a Simulated Supersonic Inlet," United Aircraft Corp., R-0920-1, East Hartford, CT, 1958.

[4]Dennard, J. S., "A Transonic Investigation of the Mass-Flow and Pressure Recovery Characteristics of Several Types of Auxiliary Air Inlets," NACA RM L57B07, Jan. 1957.

[5]Fukuda, M. K., Hingst, W. G., and Reshotko, E., "Bleed Effects on Shock/Boundary-Layer Interactions in Supersonic Mixed Compression Inlets," *Journal of Aircraft*, Vol. 14, No. 2, 1977, pp. 151–156.

[6]Wong, W. F., "The Application of Boundary Layer Suction to Suppress Strong Shock-Induced Separation in Supersonic Inlets," AIAA Paper 74-1063, Oct. 1974.

[7]Seebaugh, W., and Childs, M., "Conical Shock Wave Boundary Layer Interaction Including Suction Effects," *Journal of Aircraft*, Vol. 7, No. 4, 1970, pp. 334–340.

[8]Benhachmi, D., Greber, I., and Hingst, W., "Experimental and Numerical Investigation of an Oblique Shock-Wave/Turbulent Boundary Layer Interaction with Continuous Suction," AIAA Paper 89–0357, Jan. 1989.

[9]Hingst, W. R., and Tanji, F. T., "Experimental Investigation of Two-Dimensional Shock-Boundary Layer Interaction with Bleed," AIAA Paper 83-0135, Jan. 1973; also NASA TM-83057, Jan. 1973.

[10]Lee, D. B., and Leblanc, R., "Interaction onde de Choc Oblique-Couche Limite sur Paroi Poreuse avec Aspiration," *Improvement of Aerodynamic Performance Through Boundary Layer Control and High Lift Systems*, CP-365, AGARD, Aug. 1984 (Paper 23).

[11]Strike, W. T., and Rippy, J., "Influence of Suction on the Interaction of an Oblique Shock with a Turbulent Boundary Layer at Mach 3," Arnold Engineering Development Center, AEDC-TN-61-129, Oct. 1961.

[12]Reddy, D. R., Benson, T. J., and Weir, L. J., "Comparison of 3-D Viscous Flow Computations of Mach 5 Inlet with Experimental Data," AIAA Paper 90-0600, Jan. 1990.

[13]Paynter, G. C., Treiber, D. A., and Kneeling, W. D., "Modeling Supersonic Inlet Boundary Layer Bleed Roughness," *Journal of Propulsion and Power*, Vol. 9, No. 4, 1993, pp. 622–627.

[14]Abrahamson, K. W., and Bower, D. L., "An Empirical Boundary Condition for Numerical Simulation of Porous Plate Bleed Flows," AIAA Paper 88-0306, Jan. 1988.

[15]Cebeci, T., "Behavior of Turbulent Flow near a Porous Wall with Pressure Gradient," *AIAA Journal*, Vol. 8, No. 12, 1970, pp. 2152–2156.

[16]Cebeci, T., and Shang, K. C., "Calculation of Incompressible Rough-Wall Boundary-Layer Flows," *AIAA Journal*, Vol. 16, No. 7, 1978, pp. 730, 731.

[17]Rimlinger, M. J., Shih, T. I.-P., and Chyu, W. J., "Three-Dimensional Shock-Wave/Boundary-Layer Interactions with Bleed Through a Circular Hole," AIAA Paper 92-3084, Jan. 1992.

[18]Hamed, A., and Lehnig, T., "An Investigation of Oblique Shock/Boundary Layer/Bleed Interaction," *Journal of Propulsion and Power*, Vol. 8, No. 2, 1992, pp. 418–424.

[19]Hamed, A., and Lehnig, T., "The Effect of Bleed Configuration on Shock/Boundary Layer Interactions," AIAA Paper 91-2014, June 1991.

[20]Hamed, A., Shih, S. H., and Yeuan, J. J., "An Investigation of Shock/Turbulent Boundary Layer/Bleed Interaction," AIAA Paper 92-3085, Jan. 1992.

[21]Hamed, A., Shih, S. H., and Yeuan, J. J., "A Parametric Study of Bleed in Shock Boundary Layer Interactions," AIAA Paper 93-0294, Jan. 1993.

[22]Cooper, G. K., and Sirbaugh, J. R., "PARC Code: Theory and Usage," Arnold Engineering Development Center, AEDC-TR-89-15, Dec. 1989.

[23]Chien, K.-Y., "Prediction of Channel and Boundary-Layer Flows with a Low Reynolds Number Turbulence Model," *AIAA Journal*, Vol. 20, No. 1, 1982, pp. 33–38.

[24]Nichols, R. H., "A Two-Equation Model for Compressible Flows," AIAA Paper 90-0494, Jan. 1990.